Inclusive electron scattering on ^{3}H and ^{3}He with full inclusion of final state interactions

J. Golak,[2] H. Witała,[2] H. Kamada,[1] D. Hüber,[1] S. Ishikawa,[3] and W. Glöckle[1]
[1]*Institut für Theoretische Physik II, Ruhr Universität Bochum, D-44780 Bochum, Germany*
[2]*Institut of Physics, Jagellonian University, 30-059 Cracow, Poland*
[3]*Department of Physics, Hosei University, Chiyoda, Tokyo 102, Japan*
(Received 22 May 1995)

Inclusive electron scattering data on ^{3}He and ^{3}H are analyzed under full treatment of the final state interactions (FSI) using realistic nucleon-nucleon forces. The data are well described. We use two different methods, one where we calculate the *pd* and *ppn* breakup contributions separately and another one which is related to the optical theorem for Compton scattering. Both rely on precise solutions of Faddeev-like equations and agree perfectly. The importance of FSI and the inclusion of total isospin $T=3/2$ for the full breakup of ^{3}He is demonstrated. We also comment on the Coulomb sum rule and the extraction of the proton-proton correlation function.

PACS number(s): 21.45.+v, 21.30.+y, 25.30.Fj

I. INTRODUCTION

Inclusive electron scattering has been studied experimentally both for very light and heavier nuclei [1]. At high momentum transfers of the order of 1 GeV/*c* and above one can expect a very simple dynamical picture, namely, the virtual photon ejects just one nucleon, which due to its high momentum hardly interacts with the remaining nucleons. This leads to scaling [1]. For much lower momentum transfers of the order of a few hundred MeV/*c* rescattering of the nucleon having absorbed the photon is expected to occur. Also more complicated photon absorption mechanism on two or more nucleons (via meson exchanges) can contribute significantly. The higher momentum transfer region is theoretically not yet well under control, since general accepted and practical relativistic frameworks are still missing.

The experimental data for ^{3}He (^{3}H) for the lower momentum transfers have mostly been analyzed in the plane wave impulse approximation or including at most one pair interaction between the three nucleons in the final state [2]. Unsatisfactory descriptions resulted. Three-nucleon correlated states chosen orthogonal to the ground state lead to some success [3], though the fact that these states are not proper $3N$ scattering states dims the outcome a bit. A full inclusion of the final state interaction was achieved in [4], however, using only very simple *s*-wave *NN* forces. Nevertheless, these studies pointed clearly to the importance of FSI and led to a fair agreement with data. Technically the treatment of the full *ppn* breakup of ^{3}He (^{3}H) in [4] was performed by first calculating the $3N$ continuum states initiated by three free nucleons, which is plagued by nasty low order rescattering processes. This can be totally avoided by a different representation of the nuclear matrix element describing that full breakup, as has been shown in [5], [6]. In fact, the *pd* and *ppn* breakup of ^{3}He induced by any external probe can be calculated in "one shot" solving one and the same Faddeev-type integral equation [5–7].

Quite a different and very powerful technique, the Green's-function Monte Carlo method, has been applied also to that problem of inclusive electron scattering [8] and demonstrated even for ^{4}He, that the conventional picture of nucleon and mesonic degrees of freedom describe the data very well, if FSI is properly taken into account. Additionally a Stieltjes transform [9], [10] or possibly better an integral transform with a Lorentz kernel [11] has been tried in model systems. Applications to the $3N$ system appeared in [12] and are in preparation [13].

Here in this article we would like to use two exact methods for treating the FSI, check them against each other and compare to data [14–16], at relatively low momentum transfers, where relativity should still be of minor importance. The first method determines the *pd* and *ppn* breakup processes individually in a way which has been described in [5–7]. Thereby one determines the nuclear transition amplitudes for any kinematically complete final configuration and takes the FSI exactly into account for any type of realistic *NN* force. Thus, after appropriate integrations, all inclusive quantities like the longitudinal and transverse response functions can directly be calculated. The second formalism derived in [17] directly for inclusive electron scattering avoids the integration over all *pd* and *ppn* configurations and is related to the optical theorem for Compton scattering. Finally we add a comment on the Coulomb sum rules for ^{3}He and ^{3}H and the extraction of the proton-proton correlation function.

In Sec. II we review briefly our two methods. The results are displayed in Sec. III. We end with a brief summary and outlook in Sec. IV. The Appendix collects technical details.

II. THEORY

The standard expression for the unpolarized inclusive electron scattering cross section in the laboratory system is

$$\frac{d^3\sigma}{d\hat{k}'_0 dk'_0}=\sigma_{\mathrm{Mott}}\left\{\left(\frac{q_\mu^2}{Q^2}\right)^2 R_L(\omega,Q) + \left(\frac{-q_\mu^2}{Q^2}+\tan^2\frac{\Theta_e}{2}\right)R_T(\omega,Q)\right\}, \quad (1)$$

where ω and $Q=|\vec{Q}|$ are the energy and three-momentum of the virtual photon, Θ_e the electron scattering angle, and

$q_\mu^2=\omega^2-Q^2$, respectively. The longitudinal (R_L) and transverse (R_T) response functions result by integrating over all the nucleon degrees of freedom in the two- and three-body breakup channels of ^{3}He (^{3}H), which are not observed for inclusive scattering.

In [7] we determined numerically the exclusive cross section for pd breakup, which is composed of four structure functions and in [5], [6] in addition the cross section for ppn breakup, containing six structure functions. As a very strong and perfectly successful test for our numerics we performed the appropriate integrations over these more general expressions for the cross sections in order to arrive at the form of Eq. (1). Thereby only the structure functions W_T and W_S for both types of breakup contribute to R_T and only W_c to R_L.

The structure functions in Eq. (1) have the form

$$R_L=\frac{2}{3}M_N q_0\int d\hat{q}_0\,\frac{1}{2}\sum_{M m_d m_N}|N_0^{pd}|^2 + \frac{1}{3}M_N\int d\hat{q}\int d\hat{p}\int_0^{\sqrt{M_N E_f}}dp\,p^2 q\,\frac{1}{2}\sum_{M m_1 m_2 m_3}|N_0^{ppn}|^2 \tag{2}$$

and

$$R_T=\frac{2}{3}M_N q_0\int d\hat{q}_0\,\frac{1}{2}\sum_{M m_d m_N}(|N_+^{pd}|^2+|N_-^{pd}|^2) + \frac{1}{3}M_N\int d\hat{q}\int d\hat{p}\int_0^{\sqrt{M_N E_f}}dp\;p^2 q \times\frac{1}{2}\sum_{M m_1 m_2 m_3}(|N_+^{ppn}|^2+|N_-^{ppn}|^2). \tag{3}$$

In the above expressions we use the Jacobi momenta $\vec{q}_0$ or $\vec{p}$, $\vec{q}$ instead of the individual momenta of the nuclear fragments $\vec{p}_N$, $\vec{p}_d$ or $\vec{p}_1$, $\vec{p}_2$, $\vec{p}_3$. They are given as

$$\vec{q}_0\equiv q_0\hat{q}_0=\frac{2}{3}\left(\vec{p}_N-\frac{1}{2}\,\vec{p}_d\right),$$

$$\vec{p}\equiv p\;\;\hat{p}=\frac{1}{2}(\vec{p}_2-\vec{p}_3),$$

$$\vec{q}\equiv\sqrt{\frac{4}{3}(M_N\;E_f-p^2)}\,\hat{q}\;=\frac{2}{3}\left[\vec{p}_1-\frac{1}{2}\;(\vec{p}_2+\vec{p}_3)\right], \tag{4}$$

where M_N is the nucleon mass. In Eqs. (2) and (3) M is the initial state magnetic quantum number and m_d, m_N, m_1, m_2, m_3 are the magnetic spin quantum numbers of the final particles. Further, E_f is the internal kinetic energy in the final three-body breakup state expressed in terms of the energy and momentum transfers and the (negative) ^{3}He (^{3}H) binding energy $\epsilon_{^3\mathrm{He}}(\epsilon_{^3\mathrm{H}})$

$$E_f\;=\;\omega+\epsilon_{^3\mathrm{He}}-\frac{\vec{Q}^2}{6M_N}. \tag{5}$$

The central quantities, the nuclear matrix elements

$$N_0\;\equiv\;\langle\Psi_f^{(-)}|\rho|\Psi_{\mathrm{bound}}\rangle \tag{6}$$

and

$$N_\pm\;\equiv\;\langle\Psi_f^{(-)}|j_\pm|\Psi_{\mathrm{bound}}\rangle, \tag{7}$$

contain the ground state Ψ_{bound} of the target, the scattering eigenstates $\Psi_f^{(-)}$ of the $3N$ Hamiltonian corresponding to the two types of breakup (pd and ppn), the density operator ρ, and the spherical components $j_\pm$ of the current operator. The advantage of evaluating the response functions in this approach is that one can determine the individual contributions from the two- and three-body electrodisintegration processes. As is shown in [5–7] the nuclear matrix elements are determined as ($\kappa=0,\pm$)

$$N_\kappa=N_\kappa^{\mathrm{PWIAS}}+N_\kappa^{\mathrm{rescatt}}, \tag{8}$$

which separates the contribution from the symmetrized plane wave approximation, here denoted as PWIAS, and from all rescattering processes summed up to infinite order.

The amplitudes for PWIAS are

$$N_\kappa^{\mathrm{PWIAS}}\;=\;\begin{cases}3\langle\phi_{pd}|(1+P)j_\kappa(\vec{Q})|\Psi_{\mathrm{bound}}\rangle & \text{for } pd \text{ breakup}\\ 3\langle\phi_0\;|(1+P)j_\kappa(\vec{Q})|\Psi_{\mathrm{bound}}\rangle & \text{for } ppn \text{ breakup}\end{cases} \tag{9}$$

and for all rescattering processes

$$N_\kappa^{\mathrm{rescatt}}\;=\;\begin{cases}3\langle\phi_{pd}|P|U_\kappa\rangle & \text{for } pd \text{ breakup}\\ 3\langle\phi_0|(1+P)|U_\kappa\rangle & \text{for } ppn \text{ breakup}\end{cases} \tag{10}$$

Here U_κ obeys the Faddeev-type integral equation

$$|U_\kappa\rangle=tG_0(1+P)j_\kappa(\vec{Q})|\Psi_{\mathrm{bound}}\rangle\;+tG_0P|U_\kappa\rangle, \tag{11}$$

where t is the two-nucleon t matrix, G_0 the free $3N$ propagator, P the sum of a cyclic and anticyclic permutation of three objects, ϕ_{pd} and ϕ_0 final channel states, and $j_\kappa(\vec{Q})$ components of a single nucleon current operator. For more details of our notation and the technique to evaluate the amplitudes, see [5], [7], [18].

In comparison to nucleon-deuteron scattering, which is governed by the same integral kernel as in Eq. (11), essentially only one new structure arrives, the single nucleon current operator applied to the $3N$ ground state $|\Psi_{\mathrm{bound}}\rangle$. This building block in momentum space and partial wave decom-

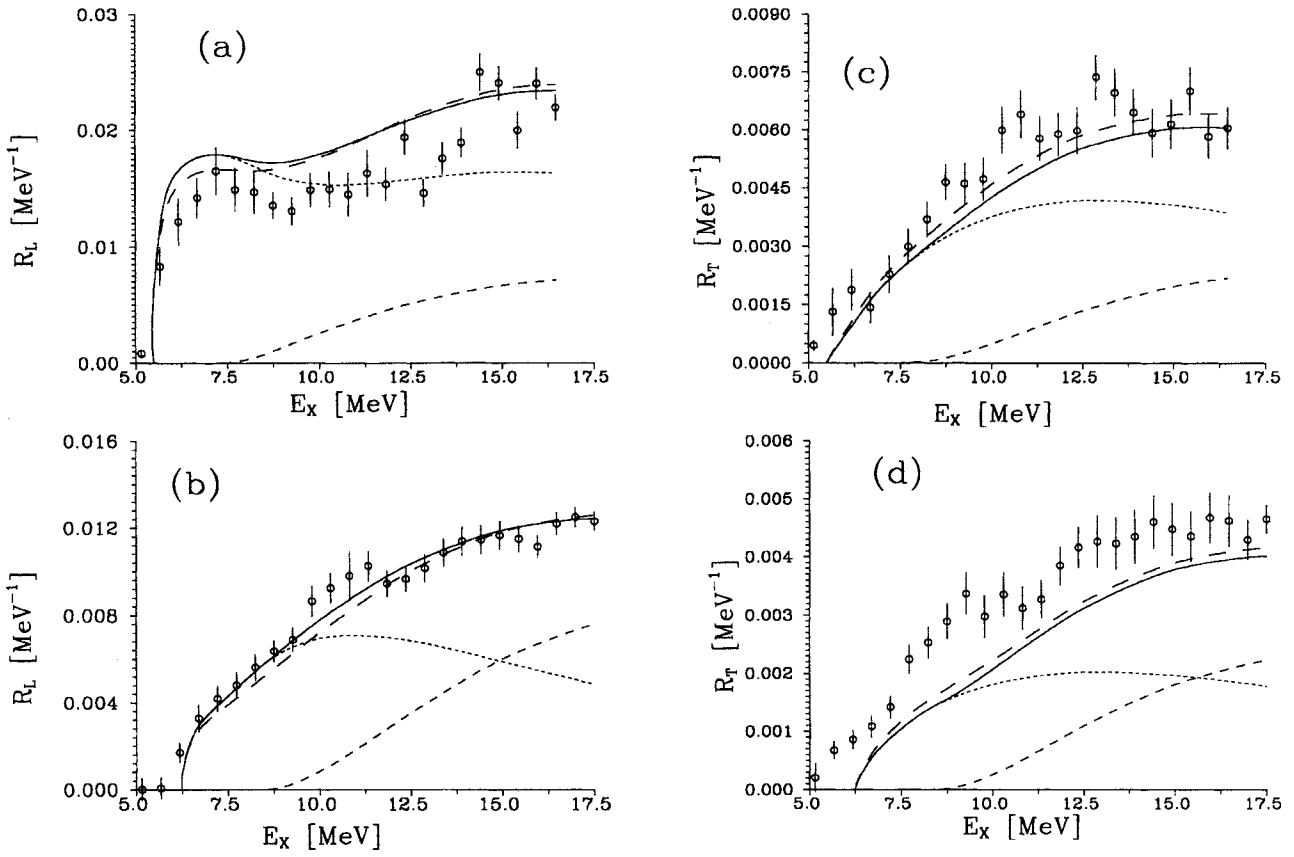

FIG. 1. (a) ^{3}He longitudinal, (b) ^{3}H longitudinal, (c) ^{3}He transverse, and (d) ^{3}H transverse response functions, respectively, at $Q=174$ MeV/c. Comparison of data [16] to full treatments of FSI using Bonn B (solid line) and MT I-III (long dashed line). Also shown are the separate contributions for Nd (short dashed) and $3N$ breakup (medium long dashed).

posed is given in the Appendix. The partial wave projected momentum space representation of the kernel can be found in [19].

Our second formulation [17] starts from the general expression for a response function related to an operator $\hat{O}$:

$$R_{\hat{O}}(\omega,Q)=-\frac{1}{\pi}\ \mathrm{Im}\langle\Psi_{\mathrm{bound}}|\hat{O}^{\dagger}\ \frac{1}{E+i\epsilon-H}\ \hat{O}|\Psi_{\mathrm{bound}}\rangle, \tag{12}$$

where H is the $3N$ Hamiltonian and $E=\omega+E_0$ the sum of the energy brought into the system: the photon energy ω and the ground state energy E_0 related to $|\Psi_{\mathrm{bound}}\rangle$. This form has been used in evaluating the longitudinal response function $R_L(\omega,Q)$ in [17]. Now we can follow the steps described in [17] also for $\hat{O}=j_{\pm}$ and arrive easily at

$$R_T(\omega,Q)=-\frac{1}{\pi}\ \mathrm{Im}\ \langle\Psi_{\mathrm{bound}}|j_+^{\dagger}(\vec{Q})(1+P)G_0(E)|U'_+\rangle - \frac{1}{\pi}\mathrm{Im}\ \langle\Psi_{\mathrm{bound}}|j_-^{\dagger}(\vec{Q})(1+P)G_0\ (E)|U'_-\rangle \tag{13}$$

where $U'_{\pm}$ obeys

$$|U'_{\pm}\rangle=\ (1+t\ G_0)\ j_{\pm}\ (\vec{Q})|\Psi_{\mathrm{bound}}\rangle\ +\ t\ G_0\ P|U'_{\pm}\rangle. \tag{14}$$

This equation (14) is obviously analogous to Eq. (12) in [17], which contains the density operator and generates the input for R_L. For the unpolarized case and using the properties of the current density operator one can simplify Eq. (13) to

$$R_T(\omega,Q)=-\frac{2}{\pi}\mathrm{Im}\langle\Psi_{\mathrm{bound}}|j_+^{\dagger}(\vec{Q})(1+P)\ \ G_0(E)|U'_+\rangle. \tag{15}$$

Obviously Eqs. (11) and (14) are very similar and the solutions are related by

$$|U_\kappa\rangle=|U'_\kappa\rangle+j_\kappa(\vec{Q})|\Psi_{\mathrm{bound}}\rangle. \tag{16}$$

Thus actually we solve Eq. (11). We obtain the solution by summing up the Neumann series using Padé.

That second method does not require the summation over all the $3N$ continuum states for both types of breakup and is insofar much superior, but one loses the insight of how the response functions are built up in detail.

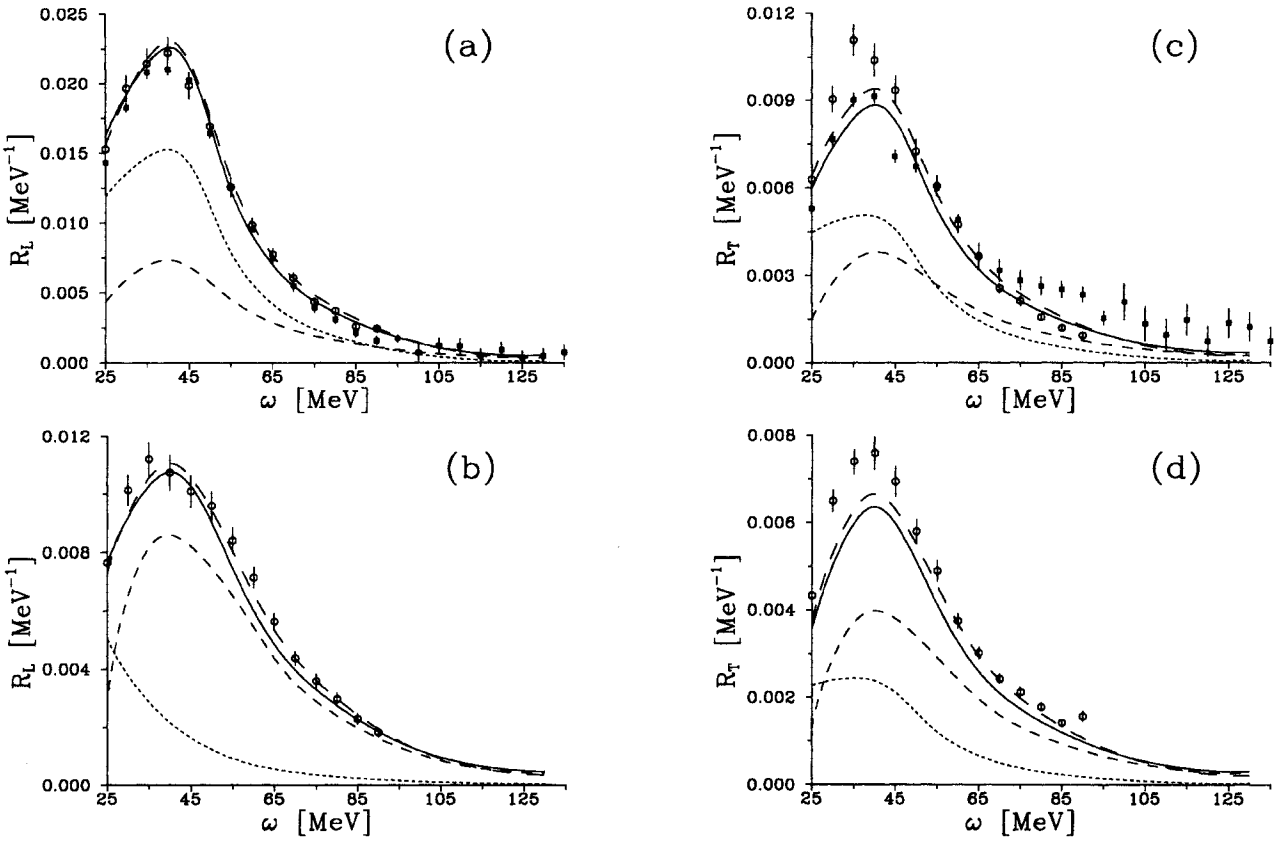

FIG. 2. (a) ^{3}He longitudinal, (b) ^{3}H longitudinal, (c) ^{3}He transverse, and (d) ^{3}H transverse response functions, respectively, at $Q=250$ MeV/c. Comparison of data [15] (circles) and [14] (squares) to full treatments of FSI using Bonn B (solid line) and MT I-III (long dashed line). Also shown are the separate contributions for Nd (short dashed) and $3N$ breakup (medium long dashed).

III. RESULTS

In this article we restrict ourselves to a single nucleon current operator in its most simple nonrelativistic form, as displayed explicitly in [7]. Consistent with that we also use strictly nonrelativistic kinematics. The electromagnetic nucleon form factors F_1 and F_2 are from Gari and Krümpelmann [20]. The initial $3N$ bound state is always based on a 34 channel Faddeev calculation. While in [17] we restricted the NN force to act in the final $3N$ continuum only in the states $^1S_0$ and $^3S_1$-$3D_1$, we include now all NN force components for total NN angular momenta up to $j=2$. The Coulomb force between the two protons is neglected.

As NN force for the study of inclusive scattering, we use the Bonn B potential [21]. From previous experience [5–7] we do not expect much dependence on the specific choice of the realistic NN force.

We analyzed data [14–16] for $Q=$ 174 MeV/c, 250 MeV/c and 300 MeV/c, where relativity should be not yet very important. We start with the analysis of recent data [16] at $Q=$ 174 MeV/c. They have been analyzed before using orthogonal correlated states for the $3N$ continuum [3] with moderate success and by a correct treatment of the three interacting nucleons [4] leading to an overall good description. In the latter case, however, only oversimplified pure s-wave NN forces, the MT I-III potential [22] have been used. It is therefore interesting to see whether a realistic NN force in all its complexity possibly modifies the theoretical outcome. We show in Fig. 1 the two structure functions for ^{3}He and ^{3}H, comparing the Bonn B and MT I-III predictions, with each other and with the data. The full calculation for R_L exhibits the well known enhancement near the pd threshold for ^{3}He and its absence for ^{3}H. The fact that the theory is slightly above the data for ^{3}He at the very low excitation energies ($E_X \equiv \omega - \tilde{Q}^2/6M_N \leq$ 10 MeV) possibly results from the neglection of the Coulomb repulsion in our treatment, which can be expected to suppress the emission of low energetic protons in reality. The agreement with the ^{3}H data is very good. We use the experimental binding energies -7.72 MeV and -8.48 MeV for ^{3}He and ^{3}H, respectively and not the theoretical ones for Bonn B, which would be -8.14 MeV for ^{3}H and the corresponding Coulomb shifted value for ^{3}He. The transverse structure function R_T is fairly well described for ^{3}He but underestimated for ^{3}H. It remains to be seen whether mesonic exchange currents are responsible for that effect. The separate contributions from the two- and three-body breakup channels to the total responses are also shown. For ^{3}He the pd channel is rather strong for obvious reasons, while the nd channel for ^{3}H is less populated and overtaken by the nnp breakup already at $E_X \approx$ 15 MeV.

Let us now regard the comparison of the two potential predictions in Fig. 1. They are surprisingly very close to each

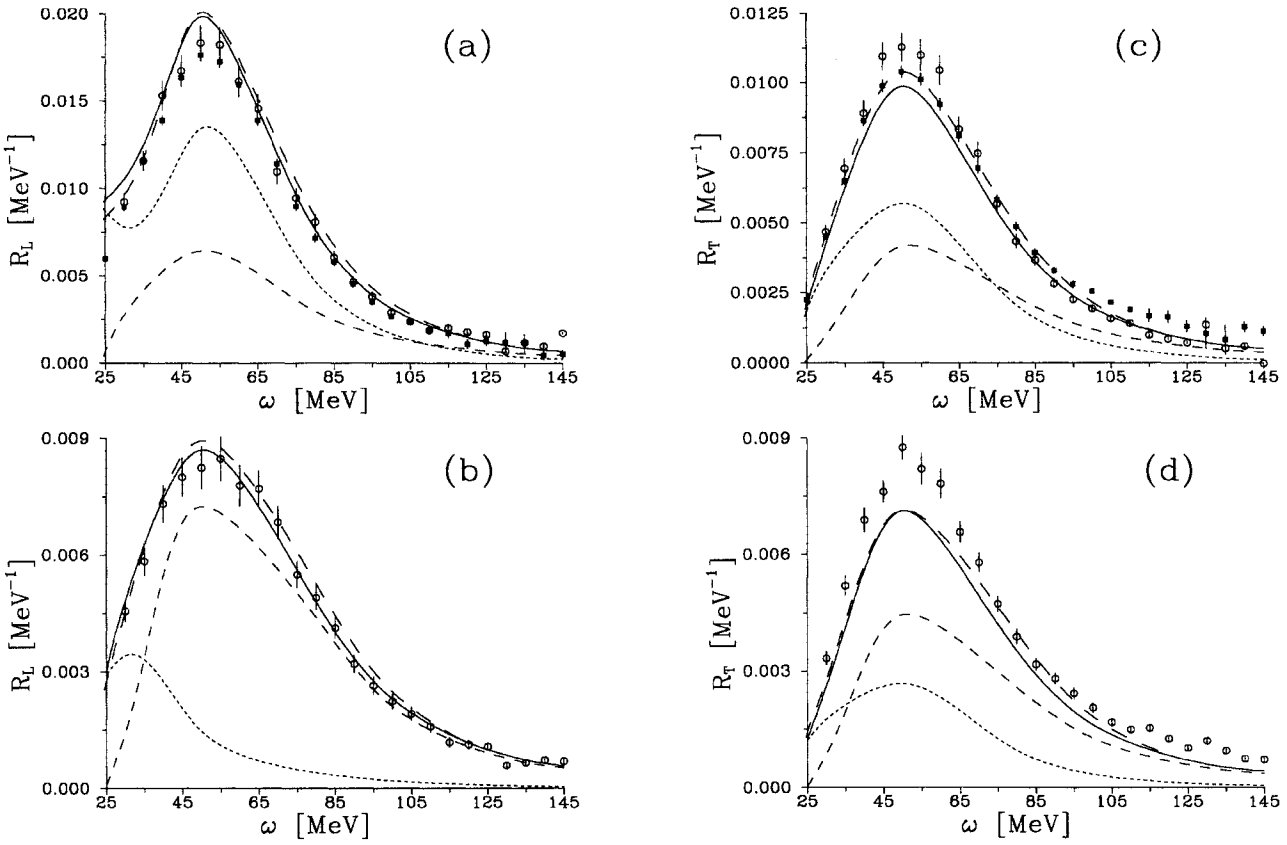

FIG. 3. The same as in Fig. 2 at $Q = 300$ MeV/c.

other. Note that the Bonn B calculation includes the NN force in the final $3N$ continuum up to $j=2$ states, whereas the MT potential is a pure s-wave interaction and has therefore not even tensor forces. Also comparing with the figures in [16] we agree quite well with the calculations of the Utrecht group, though there are differences in the treatment of the kinematics, of the current operator and also of the local MT I-III force, which is approximated in [16] by finite rank expressions, while we treat the full force. Apparently all that is of minor importance. One has to conclude that the two inclusive structure functions for the present kinematical conditions do not probe $3N$ breakup configurations, which are sensitive to the nuclear dynamics, like for instance the deuteron knockout peak [5–7], where the prediction of the MT I-III force is totally off the data. We come back to that point below.

Next we regard in Figs. 2 and 3 the two responses for ^{3}He and ^{3}H at $Q = 250$ MeV/c and 300 MeV/c, respectively. For R_L the agreement with the data is quite good, with a small overshooting for ^{3}He at 300 MeV/c. As we saw in [17] already the lowest order relativistic correction to the density operator lowers R_L in the peak by about 10 % for $Q = 300$ MeV/c. Thus a good part of that small discrepancy might in fact be due to relativistic effects. On the other hand we consider estimates of relativistic effects generated by p/m expansions with great caution [23]. The full results for R_T underestimate the data for both Q values under the peak. Unfortunately at 250 MeV/c the two sets of data [14], and [15], scatter against each other. As was shown in [8] for ^{4}He one has to expect for R_T significant contributions from two-body currents, which we have not yet included. Again the MT I-III prediction is very close to the one for Bonn B.

The separate contributions of the two- and three-body breakup to the total responses are also shown in Figs. 2 and 3. For R_L and ^{3}He the pd contribution dominates, while for R_T both contributions are comparable. For ^{3}H the nnp breakup contribution clearly dominates for R_L and to a lesser extent also for R_T.

In Fig. 4 we show the PWIAS predictions together with the full calculation for the four structure functions. This is for Bonn B and $Q = 250$ MeV/c. We see that PWIAS is totally off. Note, however, that we do not include any rescattering [see Eq. (5)] in contrast to other usage [2], [17], which take some first order corrections (not all) in the NN t matrix into account.

Since the current operator explicitly breaks isospin, one has to expect not only $T = 1/2$ but also $T = 3/2$ contributions in the final states. This is shown in Fig. 5. While for R_L and ^{3}He the $T = 3/2$ contributions are small in comparison to the ones of $T = 1/2$, they are quite significant for R_T. In the case of ^{3}H the $T = 1/2$ and $T = 3/2$ contributions are almost equal for R_T but for R_L the $T = 1/2$ contribution is again dominant but to a much lesser extent than in the case of ^{3}He. Note that the $T = 3/2$ contributions calculated at the same internal energy are equal for ^{3}He and ^{3}H separately for R_L and R_T.

Finally we display in Fig. 6 for $Q = 300$ MeV/c and ^{3}He the two response functions for various orders of rescat-

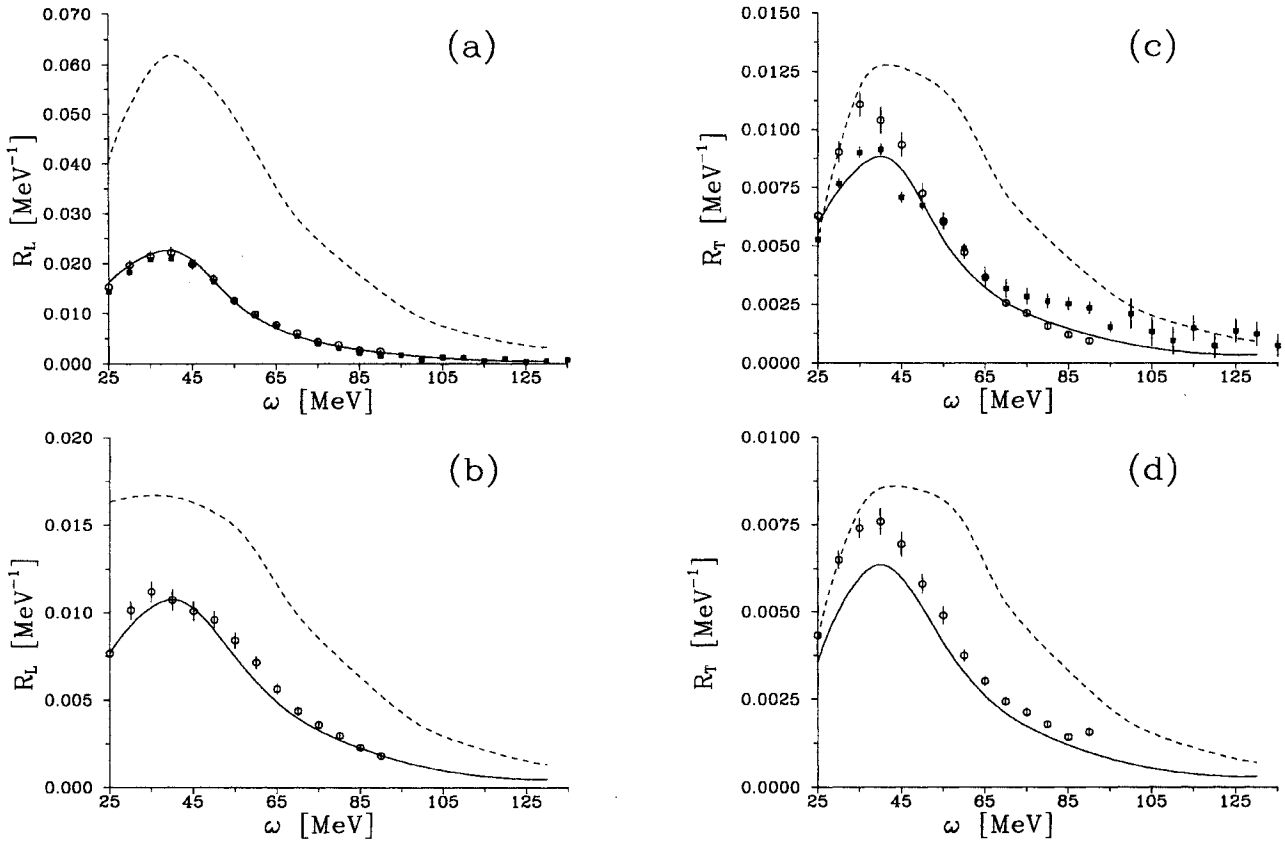

FIG. 4. (a) ^{3}He longitudinal, (b) ^{3}H longitudinal, (c) ^{3}He transversal, (d) ^{3}H transversal response functions, respectively at $Q=250$ MeV/c. The PWIAS predictions are displayed in comparison to the full Bonn B calculation and the data (see Fig. 2).

tering in the NN t matrix t. Thereby the nuclear matrix element is calculated as a sum over PWIAS and the rescattering part $N_\kappa^{\text{rescatt}}$, which is summed up to a certain order in t without using Padé. We see that for low ω values the multiple scattering series clearly diverges, while for $\omega \geq 100$ MeV rescattering beyond the second order in t is unimportant. Note that R_T evaluated in first order in t describes the data quite beautifully, a result which is obviously meaningless, however.

We have used two quite different techniques to evaluate the response functions as discussed in Sec. II. The results gained by the two methods agree within about 1%, which is our typical numerical accuracy. This is in line with our numerical experience for nucleon-deuteron scattering, where the total breakup cross section can be simply related to the optical theorem, but can also be calculated directly by integrating the fivefold differential breakup cross section over all degrees of freedom. Also there, both results agreed within 1%.

The fact that the very simplistic MT I-III s-wave potential (without tensor force) is doing about equally well as more realistic NN forces in describing the two responses led us to investigate the question of which processes dominantly feed the quasifree peaks in R_L and R_T. Looking into the expressions (2) and (3) we searched for those angles and momenta which provide the main contributions. For the pd breakup this was the quasifree peak, as expected, but because of the angular volume element carrying $\sin(\hat{q}_0 \cdot \hat{Q})$, the very peak does not contribute at all. Only the two wings contribute. The deuteron knockout peak, the description of which requires realistic NN forces (with tensor forces and higher partial waves), provides much lower cross sections and therefore is not visible in the inclusive response functions. This is illustrated in Fig. 7 for $\omega = 100$ MeV and $Q = 300$ MeV/c. The quantities $\Delta R_{L,T}$ displayed in Fig. 7 are the integrands in the $p(n)d$ parts of Eqs. (2) and (3) in relation to the integral over θ_0, the angle between $\hat{q}_0$ and $\hat{Q}$. The insets show the proton (^{3}He) and the neutron (^{3}H) angular distributions in the laboratory system for the pd and nd breakups, respectively. We see that $\theta_0 = 0$ corresponds to the maxima in the angular distributions. The arrows in the insets indicate the angular regions, where the dominant contributions to $R_{L,T}$ come from. In the case of ^{3}H, because of the small neutron F_1 form factor, ΔR_T is much bigger than ΔR_L. Also for R_L the angular region for the dominant contributions is more spread out than for R_T.

For the full breakup contributions there are many more configurations, which, in principle, could contribute to the response functions. Using Eqs. (2) and (3) we investigated all of them and found that the dominant contributions come from the proton knockout (the corresponding two proton knockout peaks) in the direction of the virtual photon (again only nearby angles are relevant because of the angular vol-

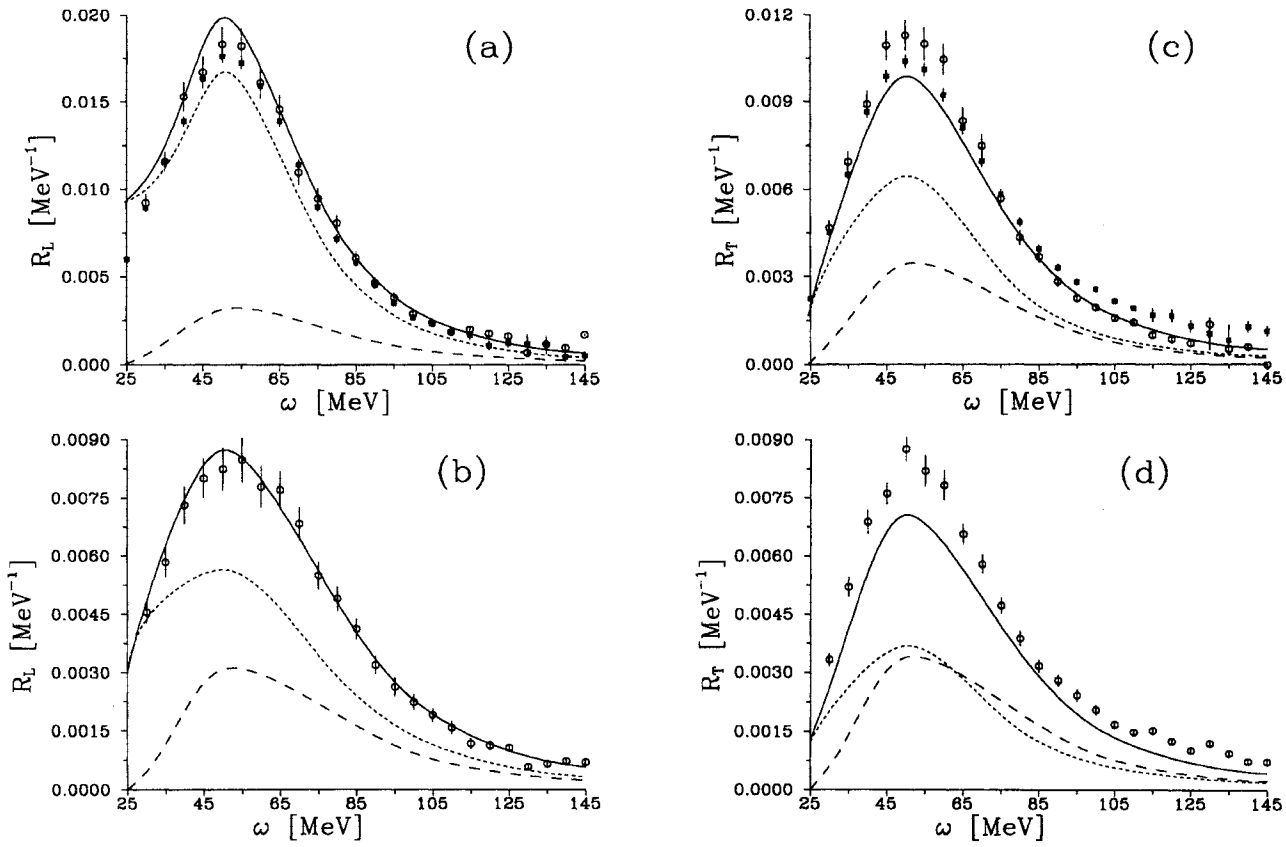

FIG. 5. The total isospin $T=1/2$ (short dashed) and $T=3/2$ (long dashed) contributions to the two responses and their sum (solid) at Q = 300 MeV/c. (a) R_L of ^{3}He, (b) R_T of ^{3}He, (c) R_L of ^{3}H, (d) R_T of ^{3}H. A similar picture arises at $Q=$ 250 MeV/c.

ume element). For R_T also the neutron knockout contributes significantly.

Since the MT potential is doing equally well as the realistic Bonn B potential, these configurations in the Nd and the full breakup cannot depend sensitively on NN force properties. In future studies we plan to search for the exclusive configurations which provide more sensitivity to NN force properties.

Finally we would like to comment on the Coulomb sum rule [24], [25] and the chance to extract the pp correlation function from it. This is an old idea and difficulties have been pointed out before [26]. The severe discrepancies found there between "experimental correlation function" and theoretical one have been removed in [27], by taking into account relativistic effects in the single nucleon density operator and on top also a two-body density operator. Both are known to contribute to the charge form factor in elastic electron scattering on ^{3}He (^{3}H), however mainly only above Q=400 MeV/c. Thus the "experimental correlation function" also depends on relativistic and two-body density contributions, which should first be subtracted before one can see the pp correlation function. Since in this article we neither include relativistic effects nor two-body densities, our comment has only two aims: we would like to point to the need for more and improved data in order to be able to extract more accurately the experimental pp correlation function and to reconfirm the failure to describe that correlation function using a single nucleon density (in nonrelativistic approximation) only and any type of modern NN force. Let us define the Coulomb sum rule by

$$S_L \equiv \frac{1}{Z}\int_{\omega_{\min}}^{\infty} R_L(\omega,Q)d\omega, \tag{17}$$

where $\omega_{\min}=-\epsilon_d+\epsilon_{^3\mathrm{He}}+Q^2/6M_N$. Using Eqs. (2), (6) and (7) and closure one arrives at

$$S_L=\frac{1}{Z}\left(\frac{1}{2}\sum_M \langle\Psi_{\text{bound}}|\rho^\dagger\rho|\Psi_{\text{bound}}\rangle - \frac{1}{2}\sum_M |\langle\Psi_{\text{bound}}|\rho|\Psi_{\text{bound}}\rangle|^2\right), \tag{18}$$

which for the single nucleon density [7] used in this article yields

$$S_L=[F_1^p(\vec{Q})]^2+\frac{N}{Z}[F_1^n(\vec{Q})]^2-ZF_{\text{ch}}^2(\vec{Q})\left(1-\frac{q_\mu^2}{4m_{^3\mathrm{He}}^2}\right) + \frac{1}{Z}\frac{3}{2}\sum_M \langle\Psi_{\text{bound}}|\rho^\dagger(1,\vec{Q})P\rho(1,\vec{Q})|\Psi_{\text{bound}}\rangle, \tag{19}$$

where

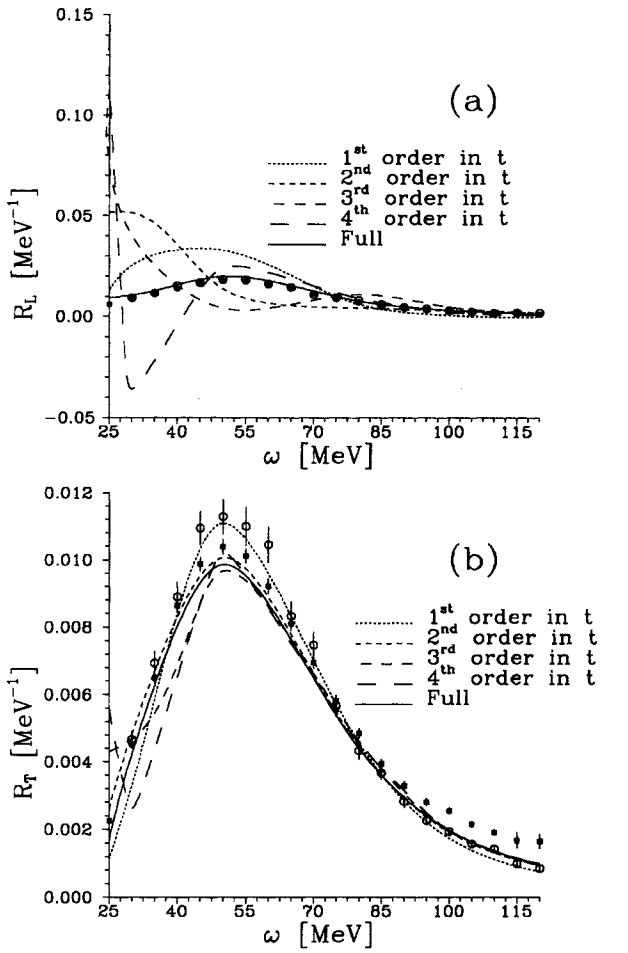

FIG. 6. The two responses for ^{3}He, (a) R_L and (b) R_T, at $Q=300$ MeV/c. Shown are the PWIAS plus different orders of rescattering in the two-nucleon t matrix t. No Padé has been used. The full calculation and the data as in Fig. 2.

$$Z^2F_{\rm ch}^2(\vec{Q})\left(1-\frac{q_\mu^2}{4m_{^3\rm He}^2}\right)\equiv\frac{1}{2}\sum_M|\langle\Psi_{\rm bound}|\rho|\Psi_{\rm bound}\rangle|^2. \tag{20}$$

The factor of 3 in the correlation term arises since the single nucleon density operator $\rho(1,\vec{Q})$ is defined to act only on one particle. The last term in Eq. (19) can easily be shown to have the explicit form

$$\frac{1}{Z}C(\vec{Q})\equiv\frac{3}{Z}\sum_M\int d\vec{p}\,d\vec{q}\langle\Psi_{\rm bound}|\vec{p}-\vec{Q},\vec{q}\rangle \times[\Pi_p(2)F_1^p(\vec{Q})+\Pi_n(2)F_1^n(\vec{Q})] \times[\Pi_p(3)F_1^p(\vec{Q})+\Pi_n(3)F_1^n(\vec{Q})]\langle\vec{p}\,\vec{q}|\Psi_{\rm bound}\rangle, \tag{21}$$

where $\Pi_{p,n}(i)$ are the projection operators on proton and neutron for particle i, respectively. The momentum shift $\vec{Q}$ in the two-body subsystem variable $\vec{p}$ makes the character of two-body correlations manifest. Note that in our theoretical treatment we always take the nucleon form factors to depend on $\vec{Q}^{\,2}$ instead of q_μ^2.

TABLE I. Information for evaluating the experimental Coulomb sum rule: the threshold values $\omega_{\rm min}$, the first experimental points in parenthesis, the $\omega_{\rm max}$ values at which extrapolation starts and the contribution of the tail in percent. The upper part (a) refers to the Bates data [15], the lower part (b) to the Saclay data [14].

Q (MeV/c)	$\omega_{\rm min}$(MeV) (^{3}He)	$\omega_{\rm max}$ (MeV)	Tail (^{3}He) [%]
	(a)		
200	12.60 (13)	45	22.7
250	16.59 (20)	90	7.8
300	21.47 (30)	125	7.0
350	27.24 (35)	135	6.6
400	33.90 (50)	160	5.8
450	41.44 (60)	190	6.6
500	49.87 (60)	195	12.6
550	59.19 (75)	240	10.7
	(b)		
250	16.59 (25)	90	5.6
300	21.47 (25)	125	5.7
350	27.24 (40)	135	8.6
400	33.90 (45)	160	9.0
450	41.44 (50)	190	8.9
500	49.87 (60)	195	17.0
550	59.19 (70)	240	15.0
600	69.40 (80)	240	23.2
650	80.49 (110)	240	45.6

Introducing the Fourier transform of the Dirac form factors

$$F(\vec{Q})\equiv\int d\vec{r}e^{i\vec{Q}\cdot\vec{r}}F(\vec{r}) \tag{22}$$

with $F^p(\vec{Q}=0)=1$ and $F^n(\vec{Q}=0)=0$ one can define a two-body correlation function

$$C(\vec{x})\equiv\frac{1}{2}\sum_M\int d\vec{r}\langle\Psi_{\rm bound}|\sum_{i\neq j}[\Pi_p(i)F_1^p(\vec{r}+\vec{x}-\hat{\vec{r}}_i) +\Pi_n(i)F_1^n(\vec{r}+\vec{x}-\hat{\vec{r}}_i)] \times[\Pi_p(j)F_1^p(\vec{r}-\hat{\vec{r}}_j)+\Pi_n(j)F_1^n(\vec{r}-\hat{\vec{r}}_j)]|\Psi_{\rm bound}\rangle. \tag{23}$$

It is normalized as

$$\int d\vec{x}C(\vec{x})=Z(Z-1), \tag{24}$$

which is just twice the number of proton pairs and generates $C(\vec{Q})$ by

$$C(\vec{Q})=\int d\vec{x}e^{i\vec{Q}\cdot\vec{x}}C(\vec{x}). \tag{25}$$

While $C(\vec{x})$ of Eq. (23) is based on extended nucleons, one can also consider the p-p correlation function for point protons

$$C^{pp}_{\text{point}}(\vec{x}) \equiv \frac{1}{2}\sum_M \int d\vec{r}\langle\Psi_{\text{bound}}|\sum_{i\neq j}\Pi_p(i)\Pi_p(j)\delta(\vec{r}+\vec{x}-\vec{r}_i)\delta(\vec{r}-\hat{\vec{r}}_j)|\Psi_{\text{bound}}\rangle$$

$$=\frac{1}{2}\sum_M \langle\Psi_{\text{bound}}|\sum_{i\neq j}\Pi_p(i)\Pi_p(j)\delta(\vec{x}-(\hat{\vec{r}}_i-\hat{\vec{r}}_j))|\Psi_{\text{bound}}\rangle. \tag{26}$$

Note that because of averaging over the magnetic quantum number M both correlation functions depend only on the magnitudes of the vectors. Using the Dirac form factors [20] we display in Fig. 8 $C(x)$ of Eq. (23) and $C^{pp}_{\text{point}}(x)$ of Eq. (26) for ^{3}He and various NN forces. While $C^{pp}_{\text{point}}(x)$ shows the well-known short range suppression, the nucleon form factors fill up the dip at short distances for $C(x)$. We see that among the potentials shown, Ruhrpot [28] and AV18 [29] (Nijmegen I [30] and Bonn B [21]) potentials have the strongest (weakest) short range repulsion. Already at around 1.5 fm the results for different potentials inside the two groups of curves essentially coincide. While $C(x)$ adds up the pp, np, and nn correlations, the pp correlations dominate by many orders of magnitudes over the other ones, which in that sum are totally negligible.

Let us now regard $C(Q)$ for various NN forces. This is displayed in Fig. 9. The small differences of $C(x)$ at short distances are reflected in small variations starting at about $Q=$ 300 MeV/c. Note that $C(Q)$ changes sign around $Q=$ 400 MeV/c. Based on the simplified assumption of a single nucleon current operator and neglecting all relativistic corrections, $C(Q)$ from Eq. (21) is related to the Coulomb sum S_L and the elastic charge form factor F_{ch} by

$$\frac{1}{Z}C(\vec{Q})=S_L-[F^p_1(\vec{Q})]^2-\frac{N}{Z}[F^n_1(\vec{Q})]^2+ZF^2_{\text{ch}}(\vec{Q})$$

$$\times\left(1-\frac{q^2_\mu}{4m^2_{^3\text{He}}}\right), \tag{27}$$

as is obvious from Eqs. (19) and (21). In the theoretical treatment the last term in Eq. (27) is evaluated according to Eq. (20). We can also use the right hand side of Eq. (27) evaluated through experimental quantities to define an experimental $C(Q)$, which might contain additional physics. In this case the last term of Eq. (27) is evaluated through the experimental charge form factor and we approximated q^2_μ by $-\vec{Q}^2$. As was discussed before [25–27], the evaluation of S_L from experimental data in Eq. (17) requires an extrapolation for the large ω values, which are not available experimentally. We followed a suggestion [31] to use an inverse power law. This is in accordance with what we found in a model study on the deuteron [32]. Here we used the expo-

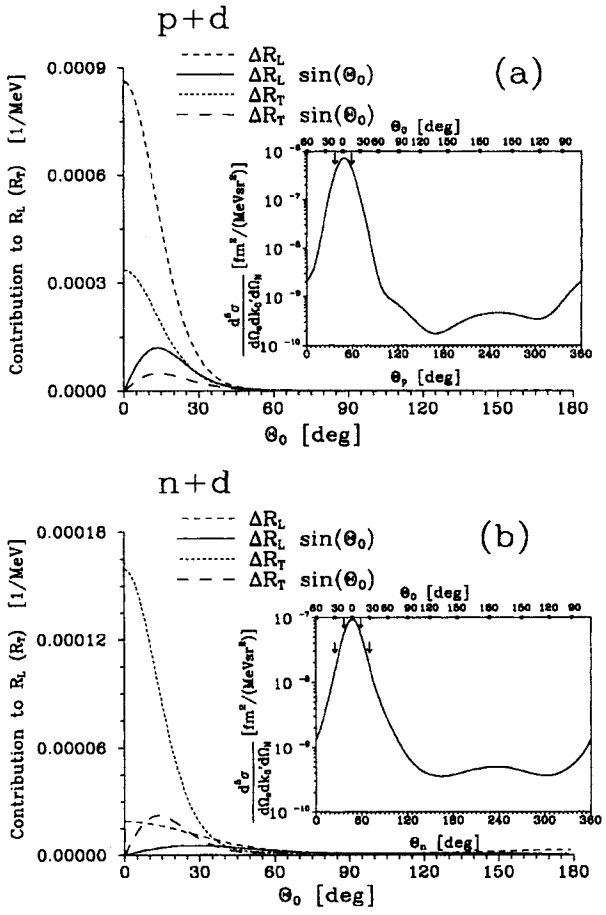

FIG. 7. (a) The $p+d$ contributions to $R_{L,T}$ (see text) together with the angular proton distribution in pd breakup of ^{3}He. The arrows in the inset indicate proton laboratory angles, where the dominant contributions come from. (b) The $n+d$ contributions to $R_{L,T}$ together with the angular neutron distribution in nd breakup of ^{3}H. The two pairs of arrows indicate the neutron laboratory angles, where the dominant contributions to R_T and R_L come from.

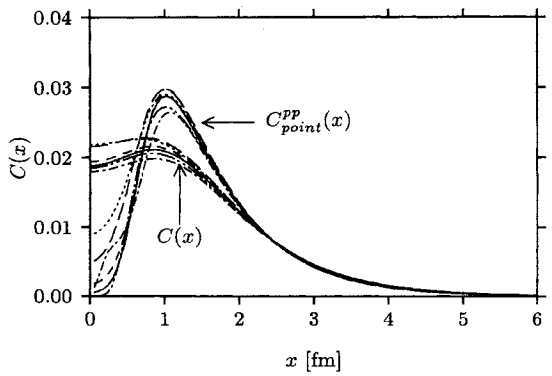

FIG. 8. The two-nucleon correlation function $C(x)$ of Eq. (23) and the point proton-proton correlation function $C^{pp}_{\text{point}}(x)$ of Eq. (26) for various NN forces: AV18 [29] (solid), Bonn B [21] (long dashed), Nijmegen 93 [30] (short dashed), Nijmegen I [30] (dotted), Paris [36] (dash-dotted) and Ruhrpot [28] (dash-double-dotted).

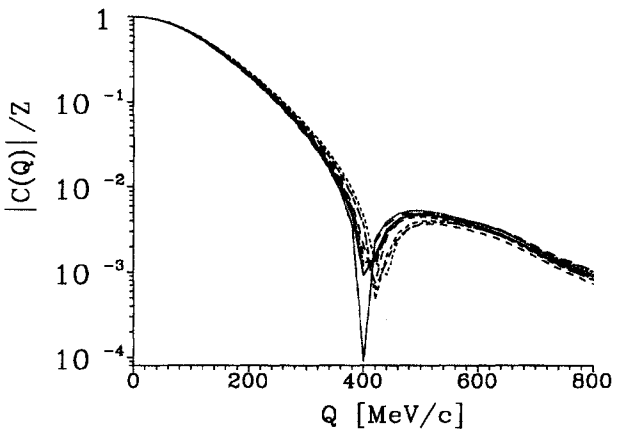

FIG. 9. The two-nucleon correlation function $|C(Q)|/Z$ of Eq. (21) for various NN forces. Description as in Fig. 8.

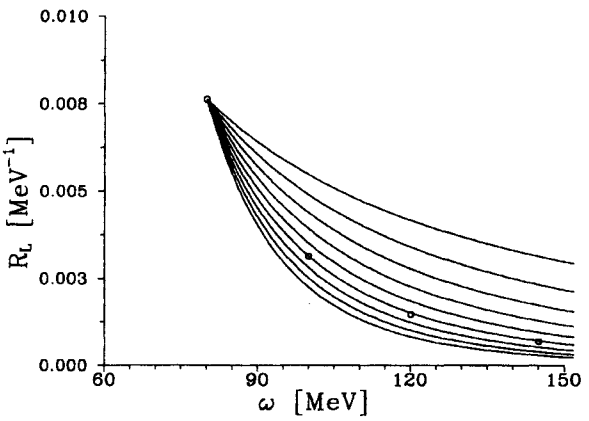

FIG. 10. The extrapolation of the theoretical longitudinal response function for $Q=300$ MeV/c according to Eq. (28). The exponent $\alpha=4$ is clearly favored over the other choices, which are $\alpha=$ 1.5, 2, 2.5, 3, 3.5, 4, 4.5, 5, 5.5, and 6 read from top to bottom. The open circles describe theoretically calculated R_L values.

nent 4. For $Q=$ 250 and 300 MeV/c our theoretical results definitely yield that exponent as is demonstrated in Fig. 10 for $Q=$ 300 MeV/c. There theory is compared to

$$R_L(\omega)=R_L(\omega_{\max})\left(\frac{\omega_{\max}}{\omega}\right)^{\alpha} \tag{28}$$

with $\omega_{\max}=80$ MeV. Clearly the curve with $\alpha=4$ fits perfectly well the three R_L values calculated theoretically. Obviously any $\omega_{\max}$ greater than 80 MeV would work equally well. We did not calculate R_L for $Q>$ 300 MeV/c and therefore do not know whether α will change with these larger Q's. In handling the experimental data now, we nevertheless used $\alpha=4$ throughout. In order to clearly define the way we arrived at the experimental S_L values we display in Table I the threshold values $\omega_{\min}$, the ω values of the first experimental point, the $\omega_{\max}$ values we have chosen for the extrapolation, and the contribution coming from the extrapolated tail in percent—and this for all data for ^{3}He. Between $\omega_{\min}$ and the first experimental point we have chosen just a triangular shape for the integration. Then the upper and lower limits of the error bars were connected by a spline interpolation up to $\omega_{\max}$ by two "wavy" curves, respectively, as shown in detail in Fig. 11, and then the integrals are performed. Regarding Fig. 11, one would like to see more data points for $Q=$ 200, 500, and 550 MeV/c, in order to be able to better judge the validity of the extrapolation used. The contribution from the tail is largest at these Q values (see Table I). The situation is similar for the Saclay data (not shown) and the relatively large and uncertain tail contributions are at $Q=$ 500 MeV/c and higher (see Table I). The resulting $S_L(Q)$'s for ^{3}He and ^{3}H are shown in Fig. 12 and have relatively large error bars. The theoretical sum rules evaluated according to Eqs. (19) and (21) using various NN forces are also shown. There is little dependence on the choice of the NN force. The agreement for ^{3}H is better than for ^{3}He. At the higher Q values ($Q>300$ MeV/c) relativistic effects should be expected, which are not incorporated in our treatment and therefore our theoretical values are only given for the purpose of a reference to a nonrelativistic treatment.

It was an excellent test for our numerics to also evaluate S_L theoretically via the integral (17). For $Q=$ 250 and 300 MeV/c, where we determined R_L, the agreement with the expression (20) was perfect. Thereby we evaluated of course the elastic charge form factor using the same nonrelativistic single nucleon density operator.

Let us now turn to the extraction of the experimental correlation function according to Eq. (27). We exhibit in Fig. 13 all the ingredients of Eq. (27) in the case of ^{3}He. We see that the sum of S_L and the elastic charge form factor nearly cancels $[F_1^p(Q)]^2$ and the difference is small with a big relative error. One can therefore expect that this small quantity, the searched for $C(Q)$, will depend sensitively on various effects (relativity and exchange currents), which below 400 MeV/c for the larger quantities like the sum rule and the elastic charge form factor are not yet so important. Thus we should not be too surprised that our theoretical $C(Q)$'s based on a single nucleon (nonrelativistic) density operator differ strongly in comparison to the experimental $C(Q)$'s, as shown in Fig. 14. The situation for ^{3}H is displayed in Figs. 15 and 16. Since the error bars on $C(Q)$ are too big, not much information can be gained and our most simple theoretical results $C(Q)=0$ is not questioned. This is similar to what has been found in [26]. Thus before pointing to a wrong nuclear Hamiltonian which would have the wrong bound state pp correlations, one has to question the assumption of a single nucleon density and its nonrelativistic treatment at $Q=300$ MeV/c and above. The failure of that assumption has been already seen in the elastic charge form factor of ^{3}He, where above 400 MeV/c data start to deviate strongly from that simple picture. In fact in [27] it was shown that inclusion of the Darwin-Foldy and spin-orbit relativistic corrections to the single nucleon charge operator eliminates most of the discrepancy for $C(Q)$; on top two-body densities show noticeable effects in the right direction. Since these lowest order relativistic effects change the nonrelativistic values, which we have calculated in the present article, by nearly an order of magnitude, they cannot be considered to be small corrections. This certainly calls for a consistent relativistic framework (including the incorporation of the electromagnetic nucleonic form factors, which were treated in [26] and [27] by different recipes), whose relativistic form

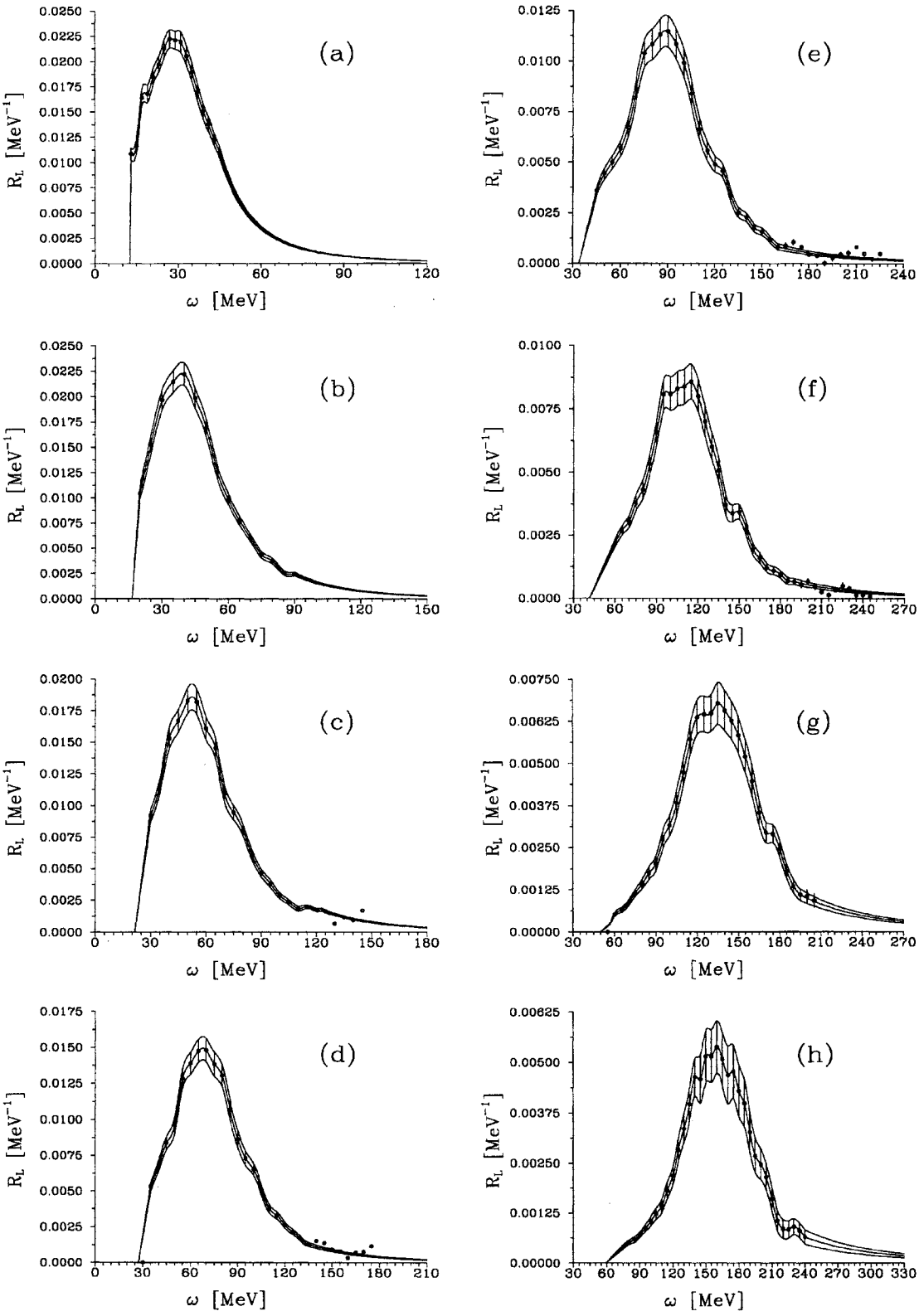

FIG. 11. The treatment of the Bates data [15] for the evaluation of S_L according to Eqs. (17) and (28). (a) $Q=$ 200 MeV/c, $\omega_{\max}=$ 45 MeV; (b) $Q=$ 250 MeV/c, $\omega_{\max}=$ 90 MeV; (c) $Q=$ 300 MeV/c, $\omega_{\max}=$ 125 MeV; (d) $Q=$ 350 MeV/c, $\omega_{\max}=$ 135 MeV; (e) $Q=$ 400 MeV/c, $\omega_{\max}=$ 160 MeV; (f) $Q=$ 450 MeV/c, $\omega_{\max}=$ 190 MeV; (g) $Q=$ 500 MeV/c, $\omega_{\max}=$ 195 MeV; and (h) $Q=$ 550 MeV/c, $\omega_{\max}=$ 240 MeV.

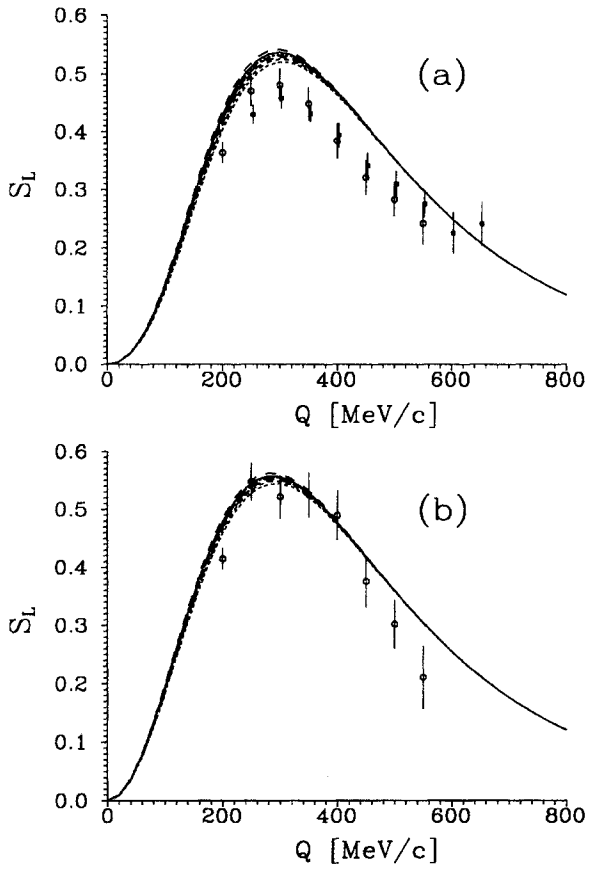

FIG. 12. The experimental Coulomb sum rule values of Eq. (17) for (a) ^{3}He based on Bates data [15] and Saclay data [14], (b) for ^{3}H based on Bates data [15]. The theoretical curves are evaluated via Eqs. (19) and (21) using various NN forces. (Description as in Fig. 8.)

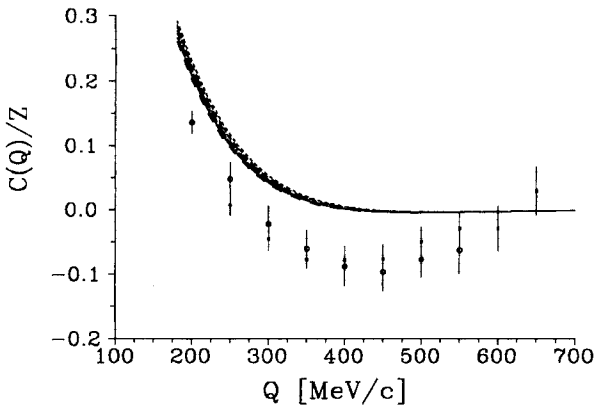

FIG. 14. Theoretical proton-proton correlation functions in ^{3}He evaluated for various NN forces (as in Fig. 8) in comparison to the experimental correlation function $C(Q)/Z$ from Fig. 13.

might change the interpretation and structure of the "correlation function." Also, additional and precise data would be needed in order to better define $C(Q)$ experimentally.

IV. SUMMARY AND OUTLOOK

We solved precisely the problem of final state interactions in the $3N$ continuum occurring in inclusive electron scattering on ^{3}He and ^{3}H using realistic NN forces. As an example we choose the Bonn B interaction.

We restricted our study to the low momentum transfers $Q=$ 174, 250, and 300 MeV/c, where we expected relativistic effects to be unimportant. In fact using the most simple nonrelativistic single nucleon current operator, the agreement for the longitudinal response with the data turned out to be rather good; the transversal response theory stays somewhat below the data, reflecting presumably the lack of two-body currents.

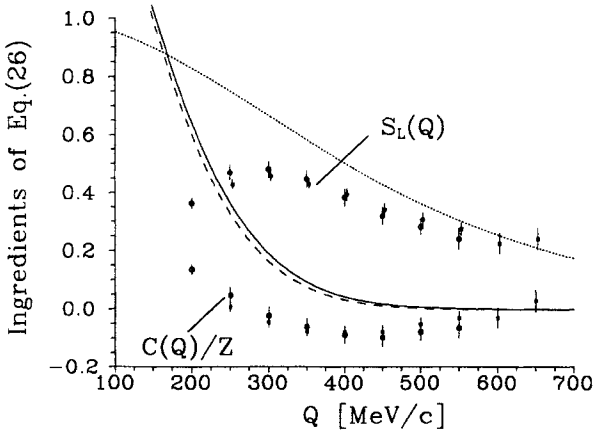

FIG. 13. The ingredients of Eq. (27) for ^{3}He: the experimental $S_L(Q)$ (open circles [15], closed squares [14]) and $[F_1^p(Q)]^2$ from [20] (dotted) and $ZF_{ch}^2(Q)(1-q_\mu^2/4M_{^3He}^2)$ (experimental values [35] (solid curve), our theoretical values (dashed curve) and $C(Q)/Z$. The term $N/Z\,(F_1^n)^2$ is totally negligible.

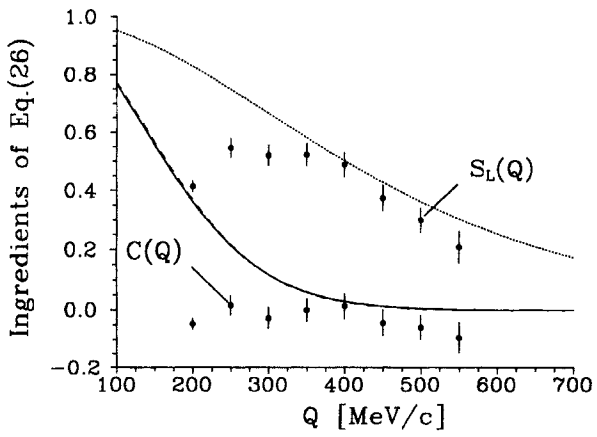

FIG. 15. The ingredients of Eq. (27) for ^{3}H : the experimental $S_L(Q)$ [15] and $[F_1^p(Q)]^2$ from [20] (dotted) and $ZF_{ch}^2(Q)\times(1-q_\mu^2/4M_{^3He}^2)$ (experimental values [35] solid curve, our theoretical values dashed curve) and $C(Q)/Z$. The term $N/Z\,(F_1^n)^2$ is totally negligible.

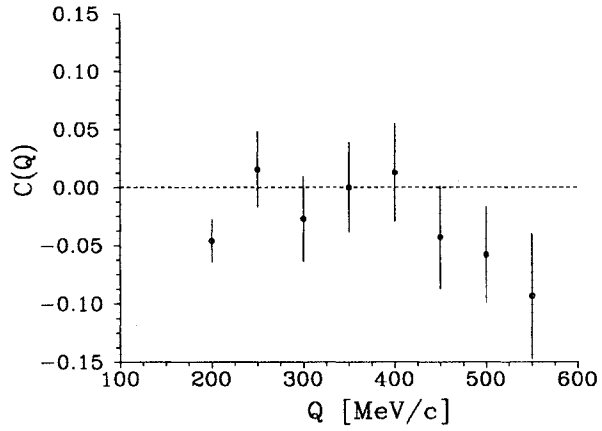

FIG. 16. The experimental correlation function $C(Q)$ for ^{3}H from Fig. 15. Our theoretical value is 0.

Then we added a comment on the Coulomb sum rule and the extraction of the pp correlation function. We pointed to the need of additional experimental information in order to reduce uncertainties in tail extrapolations and reconfirmed the failure of describing the experimental correlation function using that most simple nonrelativistic density operator. That failure is shown to occur for all NN forces presently in use. As shown in [27] relativistic corrections in the density operator and also two-body density operators appear to play an important role already at the rather low values of $Q=300$ MeV/c for that correlation function. Since the lowest order relativistic corrections displayed in [27] are not small but dominate the theoretical correlation function, a consistent relativistic framework is definitely needed in order to control that quantity conceptually.

Applications of our treatment of the $3N$ continuum to processes with polarized particles are underway and first results already appeared [33].

ACKNOWLEDGMENTS

This work was supported by the Polish Committee for Scientific Research under Grant No. PB 1031, the Science and Technology Cooperation Germany-Poland under Grant No. XO81.91, the Deutsche Forschungsgemeinschaft, and the BMFT. The numerical calculations have been performed on the Cray Y-MP of the Höchstleistungsrechenzentrum in Jülich, Germany.

APPENDIX A

We work in momentum space and use a partial wave decomposition. We refer to [34] for a detailed explanation of our notation. Our $3N$ basis states in (LS) coupling are

$$|pq\beta\rangle\equiv|pq(\ell\lambda)L(s\tfrac{1}{2})S\ \ (LS)\mathscr{J}M(t\tfrac{1}{2})TM_T\rangle. \quad \text{(A1)}$$

Alternatively to (LS) coupling, we use basis states in (jJ) coupling:

$$|pq\alpha\rangle\equiv|pq(\ell s)j\ \ (\lambda\tfrac{1}{2})J\ \ (jJ)\mathscr{J}M\ \ (t\tfrac{1}{2})TM_T\rangle. \quad \text{(A2)}$$

The two coupling schemes are simply related by

$$|pq\alpha\rangle=\sum_{LS}\sqrt{\hat{j}JLS}\begin{Bmatrix}\ell & s & j\\ \lambda & \frac{1}{2} & J\\ L & S & \mathscr{J}\end{Bmatrix}|pq\beta\rangle. \quad \text{(A3)}$$

In the above expression and in the following we use the abbreviation $\hat{a}\equiv 2a+1$.

The antisymmetry of the basis states in the two-body subsystem is imposed by the requirement

$$(-1)^{l+s+t}=-1.$$

The matrix elements of the charge density operator ρ and current densities $j_\pm\equiv j_\pm^{\rm conv}+j_\pm^{\rm spin}$ applied to the $3N$ bound state $|\Psi_{\rm bound}\rangle$ and for a fixed three-momentum transfer $\vec{Q}\|\hat{z}$, in the target rest frame are

$$\begin{aligned}\langle p'q'\beta'(\mathscr{J}'M')|\rho(\vec{Q})|\Psi_{\rm bound}(\tfrac{1}{2}\ M)\rangle\equiv&\int d\,\vec{p}\,d\,\vec{q}\langle p'q'\beta'(\mathscr{J}'M')|\vec{p}\vec{q}\rangle(\tfrac{1}{2}[1+\tau_{10}(1)]F_1^p(\vec{Q})+\tfrac{1}{2}[1-\tau_{10}(1)]F_1^n(\vec{Q}))\\ &\times\langle\vec{p},\vec{q}-\tfrac{2}{3}\vec{Q}|\Psi_{\rm bound}(\tfrac{1}{2}\ M)\rangle\\ =&\,\delta_{M,M'}\delta_{M_T,M_{T'}}\tfrac{3}{2}\sqrt{\hat{\mathscr{J}}'}\sqrt{\hat{L}'}(-1)^{S'+\mathscr{J}'}[I^{(p)}(t',T',M_T)F_1^p(\vec{Q})\\ &+I^{(n)}(t',T',M_T)F_1^n(\vec{Q})]\sum_\beta\delta_{\ell,\ell'}\delta_{s,s'}\delta_{S,S'}\delta_{t,t'}\sqrt{\hat{\lambda}\hat{L}}\sum_{\lambda_1+\lambda_2=\lambda}\sqrt{\frac{(2\lambda+1)!}{(2\lambda_1)!(2\lambda_2)!}}\\ &\times q'^{\lambda_1}(\tfrac{2}{3}\ Q)^{\lambda_2}\sum_k\hat{k}C(\lambda_1,k,\lambda';0,0,0)\int_{-1}^{1}dxP_k(x)\frac{\langle p'\tilde{q}\beta|\Psi_{\rm bound}\rangle}{\tilde{q}^\lambda}\\ &\times\sum_g\sqrt{\hat{g}}C(\lambda_2,k,g;0,0,0)\begin{Bmatrix}\lambda_2 & \lambda_1 & \lambda\\ \lambda' & g & k\end{Bmatrix}\begin{Bmatrix}\ell & \lambda' & L'\\ g & L & \lambda\end{Bmatrix}\\ &\times\begin{Bmatrix}\mathscr{J}' & L' & S'\\ L & \frac{1}{2} & g\end{Bmatrix}C(\mathscr{J}',g,\tfrac{1}{2};M',0,M), \end{aligned} \quad \text{(A4)}$$

$$\langle p'q'\beta'(\mathscr{J}'M')|j_{\pm}^{\rm conv}(\vec{Q})|\Psi_{\rm bound}(\tfrac{1}{2}\ M)\rangle \equiv \int d\ \vec{p}d\ \vec{q}\langle p'q'\beta'(\mathscr{J}'M')|\vec{p}\vec{q}\rangle(\tfrac{1}{2}[1+\tau_{10}(1)]F_1^p(\vec{Q})+\tfrac{1}{2}[1-\tau_{10}(1)]F_1^n(\vec{Q}))$$
$$\times\frac{3q_{\pm}}{M_N}\langle\vec{p},\vec{q}-\tfrac{2}{3}\ \vec{Q}|\Psi_{\rm bound}(\tfrac{1}{2}\ M)\rangle$$
$$=\frac{q'}{M_N}\delta_{M',M\pm1}\delta_{M_T,M_{T'}}\ \tfrac{3}{2}\ \sqrt{\hat{\mathscr{J}}}\sqrt{\hat{\lambda}'}\sqrt{\hat{L}'}(-1)^{S'+\mathscr{J}'}[I^{(p)}(t',T',M_T)F_1^p(\vec{Q})$$
$$+I^{(n)}(t',T',M_T)F_1^n(\vec{Q})]\sum_{\beta}\ \delta_{\ell,\ell'}\delta_{s,s'}\delta_{S,S'}\delta_{t,t'}\sqrt{\hat{\lambda}\hat{L}}\sum_{\lambda_1+\lambda_2=\lambda}\sqrt{\frac{(2\lambda+1)!}{(2\lambda_1)!(2\lambda_2)!}}$$
$$\times q'^{\lambda_1}(\tfrac{2}{3}\ Q)^{\lambda_2}\sum_k\ \hat{k}\int_{-1}^{1}dx\ P_k(x)\frac{\langle p'\tilde{q}\beta|\Psi_{\rm bound}\rangle}{\tilde{q}^{\lambda}}\sum_g\ \hat{g}C(\mathscr{J}',g,\tfrac{1}{2}\ ;M',\mp1,M)$$
$$\times\begin{Bmatrix}\mathscr{J}' & L' & S\\ L & \frac{1}{2} & g\end{Bmatrix}\begin{Bmatrix}g & L' & L\\ \ell & \lambda & \lambda'\end{Bmatrix}\sum_h\ C(\lambda_2,k,h;0,0,0)C(1,g,h;\mp1,\pm1,0)$$
$$\times\sum_f\begin{Bmatrix}\lambda_2 & \lambda_1 & \lambda\\ f & h & k\end{Bmatrix}\begin{Bmatrix}\lambda' & g & \lambda\\ h & f & 1\end{Bmatrix}C(\lambda',1,f;0,0,0)C(\lambda_1,k,f;0,0,0), \tag{A5}$$

$$\langle p'q'\alpha'(\mathscr{J}'M')|j_{\pm}^{\rm spin}(\vec{Q})|\Psi_{\rm bound}(\tfrac{1}{2}\ M)\rangle=\int d\ \vec{p}d\ \vec{q}\langle p'q'\alpha'(\mathscr{J}'M')|\vec{p}\vec{q}\rangle[\tfrac{1}{2}[1+\tau_{10}(1)]F_1^p(\vec{Q})$$
$$+\tfrac{1}{2}[1-\tau_{10}(1)]F_1^n(\vec{Q})]\ \frac{3i(\vec{\sigma}\times\vec{Q})_{\pm}}{2M_N}\langle\vec{p},\vec{q}-\tfrac{2}{3}\ \vec{Q}|\Psi_{\rm bound}(\tfrac{1}{2}\ M)\rangle$$
$$=\pm\frac{3Q}{2M_N}\sqrt{3}\delta_{M',M\pm1}\delta_{M_T,M_{T'}}\ \sqrt{\hat{\mathscr{J}}'}(-1)^{j'+J'+\mathscr{J}'}$$
$$\times(I^{(p)}(t',T',M_T)[F_1^p(\vec{Q})+2M_NF_2^p\ (\vec{Q})]+I^{(n)}(t',T',M_T)$$
$$\times[F_1^n(\vec{Q})+2M_NF_2^n\ (\vec{Q})])\ \sum_{\alpha}\ \delta_{\ell,\ell'}\delta_{s,s'}\delta_{j,j'}\delta_{t,t'}\ \sqrt{\hat{\lambda}\hat{J}}$$
$$\times\sum_{\lambda_1+\lambda_2=\lambda}\sqrt{\frac{(2\lambda+1)!}{(2\lambda_1)!(2\lambda_2)!}}q'^{\lambda_1}(\tfrac{2}{3}\ Q)^{\lambda_2}\sum_k\ \hat{k}C(\lambda_1,k,\lambda';0,0,0)\int_{-1}^{1}dxP_k(x)$$
$$\times\frac{\langle p'\tilde{q}\beta|\Psi_{\rm bound}\rangle}{\tilde{q}}\sum_g\ (-1)^gC(\lambda_2,k,g;0,0,0)\begin{Bmatrix}\lambda_2 & \lambda_1 & \lambda\\ \lambda' & g & k\end{Bmatrix}$$
$$\times\sum_f\ (-1)^f\hat{f}C(\tfrac{1}{2},f,\mathscr{J}';M',\pm1,M)C(1,f,g;\pm1,\mp1,0)$$
$$\times\begin{Bmatrix}J & J & J'\\ j & \mathscr{J}' & \frac{1}{2}\end{Bmatrix}\begin{Bmatrix}1 & g & f\\ \frac{1}{2} & \lambda' & J'\\ \frac{1}{2} & \lambda & J\end{Bmatrix}, \tag{A6}$$

with

$$\tilde{q}\equiv\sqrt{q'^2+\ \tfrac{4}{9}\ Q^2-\tfrac{4}{3}\ q'Qx}, \tag{A7}$$

$$I^{(p)}(t,T,M_T)\equiv\frac{1}{2}\ \delta_{T,\frac{1}{2}}-C(1\ \tfrac{1}{2}\ T,0M_TM_T)\sqrt{3}(-)^t\begin{Bmatrix}1 & T & \frac{1}{2}\\ t & \frac{1}{2} & \frac{1}{2}\end{Bmatrix}, \tag{A8}$$

$$I^{(n)}(t,T,M_T)\equiv\frac{1}{2}\,\delta_{T,\frac{1}{2}}+C(1\ \tfrac{1}{2}\ T,0M_TM_T)\sqrt{3}(-)^t\begin{Bmatrix}1 & T & \frac{1}{2}\\ t & \frac{1}{2} & \frac{1}{2}\end{Bmatrix}, \tag{A9}$$

$$q_\pm\equiv\hat{e}_{\pm1}\cdot\vec{q}=\sqrt{\frac{4\pi}{3}}|\vec{q}|Y_{1,\pm1}(\hat{q}). \tag{A10}$$

Here M_T is the isospin z component of the initial nucleus ($M_T=\frac{1}{2}$ for ^{3}He and $M_T=-\frac{1}{2}$ for ^{3}H).

From (A5)–(A7) we infer important properties of the current matrix elements:

$$\langle pq\beta'(\mathscr{J}',M'=\tfrac{1}{2})|\ \rho(\vec{Q})|\Psi_{\text{bound}}(\tfrac{1}{2},M=\tfrac{1}{2})\rangle\ =(-1)^{\mathscr{J}'-\frac{1}{2}+\ell'+\lambda'}\langle pq\beta'(\mathscr{J}',M'=-\tfrac{1}{2})|\ \rho(\vec{Q})|\Psi_{\text{bound}}(\tfrac{1}{2},M=-\tfrac{1}{2})\rangle, \tag{A11}$$

$$\langle pq\beta'(\mathscr{J}',M'=-\tfrac{3}{2})|\ j_-(\vec{Q})|\Psi_{\text{bound}}(\tfrac{1}{2},M=-\tfrac{1}{2})\rangle\ =(-1)^{\mathscr{J}'-\frac{1}{2}+\ell'+\lambda'}\langle pq\beta'(\mathscr{J}',M'=\tfrac{3}{2})|\ j_+(\vec{Q})|\Psi_{\text{bound}}(\tfrac{1}{2},M=\tfrac{1}{2})\rangle, \tag{A12}$$

$$\langle pq\beta'(\mathscr{J}',M'=-\tfrac{1}{2}|\ j_-(\vec{Q})|\Psi_{\text{bound}}(\tfrac{1}{2},M=\tfrac{1}{2})\rangle\ =(-1)^{\mathscr{J}'-\frac{1}{2}+\ell'+\lambda'}\langle pq\beta'(\mathscr{J}',M'=\tfrac{1}{2})|\ j_+(\vec{Q})|\Psi_{\text{bound}}(\tfrac{1}{2},M=-\tfrac{1}{2})\rangle. \tag{A13}$$

[1] For a recent review see B. D. Day, J. S. McCarthy, T. W. Donnelly, and I. Sick, Annu. Rev. Nucl. Sci. **40**, 357 (1990).

[2] H. Meier-Hajduk, C. H. Hajduk, P. U. Sauer, and W. Theis, Nucl. Phys. **A395**, 332 (1983); C. Ciofi degli Atti, E. Pace, and G. Salme, Phys. Lett. **127B**, 303 (1983); J. M. Laget, Phys. Lett. **151B**, 325 (1985).

[3] R. Schiavilla, V. R. Pandharipande, and R. B. Wiringa, Nucl. Phys. **A449**, 219 (1986); R. Schiavilla, Phys. Lett. B **218**, 1 (1989).

[4] E. van Meijgaard and J. A. Tjon, Phys. Lett. B **228**, 307 (1989); Phys. Rev. C **45**, 1463 (1992).

[5] J. Golak, H. Kamada, H. Witała, W. Glöckle, and S. Ishikawa, Phys. Rev. C **51**, 1638 (1995).

[6] W. Glöckle, J. Golak, H. Kamada, S. Ishikawa, and H. Witała, in *Proceedings of Workshop on Electron-Nucleus Scattering*, EIPC, Italy, 1993, edited by O. Benhar, A. Fabrocini, and R. Schiavilla (World Scientific, Singapore, 1994), p. 64.

[7] S. Ishikawa, H. Kamada, W. Glöckle, J. Golak, and H. Witała, Nuovo Cimento A **107**, 305 (1994).

[8] J. Carlson and R. Schiavilla, Few-Body Systems Suppl. **7**, 349 (1994).

[9] V. D. Efros, Sov. J. Nucl. Phys. **41** (1985) 949.

[10] V. D. Efros, W. Leidemann, and G. Orlandini, Few-Body System **14**, 15 (1993).

[11] V. D. Efros, W. Leidemann, and G. Orlandini, Phys. Lett. B **338**, 130 (1994).

[12] V. Y. Dobretsov, V. D. Efros, and B. Shao, Phys. At. Nucl. (to be published).

[13] S. Martinelli, H. Kamada, G. Orlandini, and W. Glöckle (unpublished).

[14] C. Marchand, P. Barreau, M. Bernheim, P. Bradu, G. Fournier, Z. E. Meziani, J. Miller, J. Morgenstern, J. Picard, B. Saghai, S. Turck-Chieze, P. Vernin, and M. K. Brussel, Phys. Lett. B **153**, 29 (1985).

[15] K. Dow, S. Dytman, D. Beck, A. Bernstein, K. I. Blomqvist, H. S. Caplan, D. Day, M. Deady, P. Demos, W. Dodge, G. Dodson, M. Farkhondeh, J. Flanz, K. Giovanetti, R. Goloskie, E. L. Hallin, E. Knill, S. Kowalski, J. W. Lightbody, Jr., R. Lindgren, X. K. Maruyama, J. McCarthy, B. Quinn, G. A. Retzlaff, W. W. Sapp, C. P. Sargent, D. M. Skopik, I. The, D. Tieger, W. Turchinetz, T. S. Ueng, N. Videla, K. von Reden, R. R. Whitney, and C. F. Williamson, Phys. Rev. Lett. **61**, 1706 (1988).

[16] G. A. Retzlaff, H. S. Caplan, E. L. Hallin, D. M. Skopik, D. Beck, K. I. Blomqvist, G. Dodson, K. Dow, M. Farkhondeh, J. Flanz, S. Kowalski, W. W. Sapp, C. P. Sargent, D. Tieger, W. Turchinetz, C. F. Williamson, W. Dodge, X. K. Maruyama, J. W. Lightbody, Jr., R. Goloskie, J. McCarthy, T. S. Ueng, R. R. Whitney, B. Quinn, S. Dytman, K. von Reden, R. Schiavilla, and J. A. Tjon, Phys. Rev. C **49**, 1263 (1994) and private communication.

[17] S. Ishikawa, H. Kamada, W. Glöckle, J. Golak and H. Witała, Phys. Lett. B **339**, 293 (1994).

[18] H. Kamada, W. Glöckle, and J. Golak, Nuovo Cimento A **105**, 1435 (1994).

[19] H. Witała, W. Glöckle, and Th. Cornelius, Few-Body Systems **3**, 123 (1988).

[20] M. Gari and W. Krümpelmann, Phys. Lett. **173B**, 10 (1986).

[21] R. Machleidt, Adv. Nucl. Phys. **19**, 189 (1989).

[22] R. A. Malfliet and J. A. Tjon, Nucl. Phys. **A127**, 161 (1969); R. A. Malfliet and J. A. Tjon, Ann. Phys. (N.Y.) **61**, 425 (1970).

[23] W. Glöckle, T. S. H. Lee, and F. Coester, Phys. Rev. C **33**, 709 (1986); L. Müller, Nucl. Phys. **A360**, 331 (1981).

[24] K. W. McVoy and L. van Hove, Phys. Rev. **125**, 1034 (1962).

[25] R. Schiavilla, A. Fabrocini, and V. R. Pandharipande, Nucl. Phys. **A473**, 290 (1987); R. Schiavilla, D. S. Lewart, V. R. Pandharipande, S. C. Pieper, R. B. Wiringa, and A. Fantoni, *ibid* **A473**, 267 (1987); R. Schiavilla, V. R. Pandharipande, A. Fabrocini, Phys. Rev. C **40**, 1484 (1989); see also a recent review, G. Orlandini, in *Proceedings of the International Conference on Physics of Few-Body and Quark-Hadronic Systems*, Kharkov, Ukraine, 1992, edited by V. Boldyshev, V. Kotlyar, and A. Shebeko (KFTI, Kharkov, 1994), p. 225.

[26] D. H. Beck, Phys. Rev. Lett. **64**, 268 (1990).
[27] R. Schiavilla, R. B. Wiringa, and J. Carlson, Phys. Rev. Lett. **70**, 3856 (1993).
[28] D. Plümper, J. Flender, and M. F. Gari, Phys. Rev. C **49**, 2370 (1994).
[29] R. B. Wiringa, V. G. J. Stoks, and R. Schiavilla, Phys. Rev. C **51**, 38 (1995).
[30] V. G. J. Stoks, R. A. M. Klomp, C. P. F. Terheggen, and J. J. de Swart, Phys. Rev. C **49**, 2950 (1994).
[31] R. Schiavilla (private communication).
[32] D. Hüber, W. Glöckle, and A. Bömelberg, Phys. Rev. C **42**, 2342 (1990).
[33] S. Ishikawa, H. Kamada, W. Glöckle, J. Golak, and H. Witała, in The IV International Symposium on Weak and Electromagnetic Interactions in Nuclei, Osaka, 1995, (unpublished).
[34] W. Glöckle, *The Quantum Mechanical Few-Body Problem* (Springer, Berlin-Tokyo, 1983).
[35] A. Amroum, V. Breton, J.-M. Cavedon, B. Frois, D. Goutte, F. P. Juster, Ph. Leconte, J. Martino, Y. Mizuno, X.-H. Phan, S. K. Platchkov, I. Sick, and S. Williamson, Nucl. Phys. **A579**, 596 (1994).
[36] M. Lacombe, B. Loiseau, J. M. Richard, R. Vinh Mau, J. Côté, P. Pirès, and R. de Tourreil, Phys. Rev. **C 21**, 861 (1980).